Journal of Solid State Chemistry 183 (2010) 1120–1126

Contents lists available at ScienceDirect

Journal of Solid State Chemistry

journal homepage: www.elsevier.com/locate/jssc

Effects of Rh on the thermoelectric performance of the *p*-type $Zr_{0.5}Hf_{0.5}Co_{1-x}Rh_xSb_{0.99}Sn_{0.01}$ half-Heusler alloys

Pramathesh Maji [a,b], Nathan J. Takas [a], Dinesh K. Misra [a], Heike Gabrisch [a,b], Kevin Stokes [a,c], Pierre F.P. Poudeu [a,b,*]

[a] The Advanced Materials Research Institute, University of New Orleans, New Orleans, LA 70148, USA
[b] Department of Chemistry, University of New Orleans, New Orleans, LA 70148, USA
[c] Department of Physics, University of New Orleans, New Orleans, LA 70148, USA

ARTICLE INFO

Article history:
Received 24 December 2009
Received in revised form
8 March 2010
Accepted 14 March 2010
Available online 18 March 2010

keywords:
Thermoelectric material
Phonon Scattering
Thermal conductivity
Half-Heusler compounds

ABSTRACT

We show that Rh substitution at the Co site in $Zr_{0.5}Hf_{0.5}Co_{1-x}Rh_xSb_{0.99}Sn_{0.01}$ ($0 \le x \le 1$) half-Heusler alloys strongly reduces the thermal conductivity with a simultaneous, significant improvement of the power factor of the materials. Thermoelectric properties of hot-pressed pellets of several compositions with various Rh concentrations were investigated in the temperature range from 300 to 775 K. The Rh "free" composition shows *n*-type conduction, while Rh substitution at the Co site drives the system to *p*-type semiconducting behavior. The lattice thermal conductivity of $Zr_{0.5}Hf_{0.5}Co_{1-x}Rh_xSb_{0.99}Sn_{0.01}$ alloys rapidly decreased with increasing Rh concentration and lattice thermal conductivity as low as 3.7 W/m*K was obtained at 300 K for $Zr_{0.5}Hf_{0.5}RhSb_{0.99}Sn_{0.01}$. The drastic reduction of the lattice thermal conductivity is attributed to mass fluctuation induced by the Rh substitution at the Co site, as well as enhanced phonon scattering at grain boundaries due to the small grain size of the synthesized materials.

Published by Elsevier Inc.

1. Introduction

Widespread interest in renewable energies has been triggered by growing global energy needs, prospects of climate change and eventual fossil fuel depletion. Among many other renewable energy technologies such as solar, wind, biomass, etc., energy production from heat sources via the use of thermoelectric materials has received tremendous attention primarily because of the abundance of thermal energy sources which can come from sunlight, from combustion of fossil fuels or from various chemical reactions as well as nuclear decay [1]. In order to create thermoelectric devices with high energy conversion efficiency, both *n*-type and *p*-type materials with large dimensionless figure of merit, $ZT=S^2\sigma T/\kappa$ (where S is the thermopower, σ is the electrical conductivity, κ is the thermal conductivity and T is the absolute temperature) within the temperature range of interest must be identified [2]. Half-Heusler alloys with a valence electron count (VEC) of 18 have demonstrated excellent potential as materials for high temperature power generation, mainly because of their large thermopower and moderately high electrical conductivity [3–9]. However, most efforts have so far been concentrated on the optimization of the thermoelectric performance of *n*-type half-Heusler alloys [3–8]. The search for promising *p*-type half-Heusler materials which can be coupled to existing high performance *n*-type half-Heusler alloys for high temperature thermoelectric power generation has only been initiated in the past decade. For example, the half-Heusler phases (VEC=18) with composition *M*CoSb (*M*=Ti, Zr, Hf) [10], ErNiSb [11], *RE*(Pd,Pt)(Bi,Sb) (*RE*=rare earth) [12–15] have been investigated as candidates for bulk *p*-type thermoelectric materials. Although the *M*CoSb (*M*=Ti, Zr, Hf) materials were found to exhibit *n*-type semiconducting behavior at room temperature [10], robust *p*-type materials can be identified in these systems with proper substitution and doping at M, Co and/or Sb sites. For instance, Sn doping at the Sb site in TiCoSb resulted in a maximum thermopower value of +222 μV/K at 840 K [16]. A similar result was reported in ZrCoSb where 10% Sn substitution at the Sb site changed the room temperature thermopower value from −8 μV/K to +130 μV/K. [10] Furthermore, substitutions between Ti, Zr and Hf at the M site in *M*CoSb half-Heusler compounds have been shown to reduce the lattice thermal conductivity [10,17]. Recently, simultaneous substitutions at both M and Sb sites in *M*CoSb compounds have generated *p*-type half-Heusler phases with improved figures of merit. For example, in the $Zr_{1-x}Ti_xCoSn_ySb_{1-y}$ family of compounds, thermal conductivity values as low as 4.5 W/m*K and a figure of merit as high as $ZT\sim0.2$ were observed at 1000 K [18]. An even larger figure of merit, $ZT\sim0.5$ at 1000 K was recently reported in the $Zr_{0.5}Hf_{0.5}CoSb_{0.8}Sn_{0.2}$ [19].

* Corresponding author. Fax: +1 504 280 3185.
E-mail address: ppoudeup@uno.edu (P.F.P. Poudeu).

0022-4596/$ - see front matter Published by Elsevier Inc.
doi:10.1016/j.jssc.2010.03.023

In this paper, we explore the effect of Rh substitution at the Co site, on the electrical conductivity, thermopower and thermal conductivity of the *p*-type $Zr_{0.5}Hf_{0.5}Co_{1-x}Rh_xSb_{0.99}Sn_{0.01}$ materials. Although high figure of merit was reported for compositions with higher Sn concentration, such compositions severely depart from the basic valence electron count of 18. In order to fully understand the effect of Rh substitution at the Co site on the thermal conductivity of the $Zr_{0.5}Hf_{0.5}Co_{1-x}Rh_xSb$ materials and determine the Rh concentration of minimum thermal conductivity, we have selected low Sn-doped compositions for this study. Thermoelectric properties of several compositions were measured in the temperature range from 300 to 775 K. Although Rh substitution at the Co site is primarily expected to reduce the lattice thermal conductivity of the materials due to large mass fluctuation and strain fluctuation field effects [20], we show that significant enhancement of the electrical conductivity as well as the thermopower toward *p*-type semiconducting behavior is achieved for optimum Rh concentrations. All compositions exhibited remarkable reduction of the lattice thermal conductivity. For example, lattice thermal conductivity as low as 3.7 W/m*K was observed at 300 K for $Zr_{0.5}Hf_{0.5}RhSb_{0.99}Sn_{0.01}$.

2. Experimental procedure

$Zr_{0.5}Hf_{0.5}Co_{1-x}Rh_xSb_{0.99}Sn_{0.01}$ half-Heusler materials ($0 \le x \le 1$) used in this study were synthesized as polycrystalline fine powders by combining elements in the desired stoichiometry via high temperature solid state reaction. Approximately 10 g of a mixture of starting materials were used for the synthesis. High purity elements (Zr: 99.7%, CERAC; Hf 99.8%, CERAC; Co: 99.5%, Alfa Aesar; Rh: 99.9%, Sigma Aldrich; Sb: 99.5%, CERAC; and Sn: 99.9%, CERAC) in their powder form, weighed under Ar atmosphere in a dry glove box were thoroughly ground into a homogeneous mixture using an agate mortar and pestle. The mixture was sealed in a fused-silica tube under a residual pressure of $\sim 10^{-4}$ Torr and heated stepwise to 1173 K using a programmable temperature tube furnace. A complete reaction could be achieved in either a one- or a two-step process. In the first heating cycle, the mixture of starting materials was slowly heated to 573 K and annealed for 24 h to prevent volatilization of low melting Sn upon rapid increase of the furnace temperature to 1173 K. The furnace temperature was held at 1173 K for 72 h followed by fast cooling to room temperature. The resulting product was well ground under Ar atmosphere in a dry glove box and sealed in a fused-silica tube under residual pressure of $\sim 10^{-4}$ Torr for the second heating cycle. The furnace temperature was rapidly raised to 1173 K, annealed for an additional 72 h and finally rapidly cooled to room temperature. Upon completion of the reaction, the final powder was sieved and only powders with particles sizes less than 20 μm were used in subsequent characterization steps. To check the purity of the synthesized materials, powder X-ray diffraction (PXRD) patterns were measured using a PANalytical X'pert Pro X-ray diffraction system equipped with a curved graphite crystal monochromator and a scintillation counter. The system was operated in $\theta-\theta$ geometry, using Cu$K\alpha$ radiation and tube settings of 40 kV and 40 mA. Data were acquired from 15° to 75° in 2θ. Specimens for electrical conductivity, thermopower and thermal conductivity measurements were fabricated by hot pressing fine powders of the half-Heusler materials using a 10-ton uniaxial hot press system. The pressing was carried out under dynamic vacuum of $\sim 10^{-4}$ Torr. Pellets were obtained by applying a maximum pressure of 100 MPa with the furnace temperature set to 1173 K. Relative density of the pressed pellets used for thermoelectric properties measurements are summarized in Table 1 along with lattice parameter, bulk density, and room temperature lattice thermal conductivity of selected compositions. The resulting pellets were polished into disk-shaped specimens with approximate thickness of 2.5 mm and diameter of 10 mm for thermal diffusivity measurements. Rectangular bar specimens with approximate dimensions 3.0 mm × 2.5 mm × 9 mm for simultaneous measurement of the electrical conductivity and thermopower were also cut from the same pellets using a wire saw. All specimens were polished with SiC sandpaper to a mirror-like finish. Densities of powders and pressed pellets were respectively obtained by He gas pycnometry using a Micromeritics Accupyc II 1340 and by geometrical measurements using a digital micrometer. Thermal diffusivity was measured using a Netzsch LFA 457 laser flash system. A pyroceram reference material was measured alongside each sample. Measurements were made under flowing N_2 gas (> 30 mL/min) from 300 to 775 K at increments of 25 K. Cp values for thermal conductivity calculations were extracted from the laser flash data. Electrical conductivity and thermopower measurements were performed simultaneously using a commercial ZEM-3 electrical properties measurement system manufactured by Ulvac. To ensure reproducibility, data were collected on three heating and cooling cycles under a residual pressure of He gas, over the range from 300 to 775 K at increments of 25 K, using ΔT values of 5, 10 and 15 K for all temperature steps. The compositions of specimens used for the thermoelectric properties measurements were confirmed by energy dispersive spectroscopy (EDS).

3. Results and discussion

Fine powders of $Zr_{0.5}Hf_{0.5}Co_{1-x}Rh_xSb_{0.99}Sn_{0.01}$ half-Heusler alloys were synthesized at 90% to 95% purity using traditional solid state

Table 1
Lattice parameter, bulk density (He gas pycnometric), relative density of hot pressed pellets and room temperature lattice thermal conductivity of selected $Zr_{0.5}Hf_{0.5}Co_{1-x}Rh_xSb_{0.99}Sn_{0.01}$ half-Heusler alloys.

Nominal composition	Lattice parameter (Å)	Bulk density (g/cm^3)	Relative pellets density (%)	$\kappa_{lattice}$ (W/mK) at 300 K
$Zr_{0.5}Hf_{0.5}CoSb_{0.99}Sn_{0.01}$	6.0489(3)	9.176(2)	97	6.25(2)
$Zr_{0.5}Hf_{0.5}Co_{0.9}Rh_{0.1}Sb_{0.99}Sn_{0.01}$	6.0899(2)	9.222(3)	99	5.23(1)
$Zr_{0.5}Hf_{0.5}Co_{0.8}Rh_{0.2}Sb_{0.99}Sn_{0.01}$	6.0905(4)	9.255(3)	90	4.432(7)
$Zr_{0.5}Hf_{0.5}Co_{0.7}Rh_{0.3}Sb_{0.99}Sn_{0.01}$	6.1201(2)	9.332(3)	96	5.150(4)
$Zr_{0.5}Hf_{0.5}Co_{0.6}Rh_{0.4}Sb_{0.99}Sn_{0.01}$	6.1295(3)	–	–	–
$Zr_{0.5}Hf_{0.5}Co_{0.5}Rh_{0.5}Sb_{0.99}Sn_{0.01}$	6.1579(1)	9.365(4)	–	–
$Zr_{0.5}Hf_{0.5}Co_{0.4}Rh_{0.6}Sb_{0.99}Sn_{0.01}$	6.1762(3)	9.472(3)	96	4.57(2)
$Zr_{0.5}Hf_{0.5}Co_{0.3}Rh_{0.7}Sb_{0.99}Sn_{0.01}$	6.1960(3)	–	–	–
$Zr_{0.5}Hf_{0.5}Co_{0.2}Rh_{0.8}Sb_{0.99}Sn_{0.01}$	6.2284(2)	9.494(3)	–	–
$Zr_{0.5}Hf_{0.5}Co_{0.1}Rh_{0.9}Sb_{0.99}Sn_{0.01}$	6.2316(1)	9.633(4)	96	4.30(2)
$Zr_{0.5}Hf_{0.5}Rh_{1.0}Sb_{0.99}Sn_{0.01}$	6.2404(1)	9.691(4)	99	3.767(5)

reaction at 1173 K. Complete reaction of the starting elements could be achieved within a week without the need for ultra-high temperature processes such as arc-melting and induction melting, typically used for the synthesis of half-Heusler alloys. Control over the composition of the resulting half-Heusler materials is limited with these methods. Furthermore, the ingots resulting from arc-melting and induction melting are often not homogenous and usually require long annealing at high temperature to complete the reaction. The traditional solid state synthetic technique used in this study not only provided better control over the composition of the final product, but ultra-fine powders of the desired $Zr_{0.5}Hf_{0.5}Co_{1-x}Rh_xSb_{0.99}Sn_{0.01}$ materials could also be obtained.

The X-ray powder diffraction patterns (Fig. 1A) indicated complete substitution of Co by Rh in $Zr_{0.5}Hf_{0.5}Co_{1-x}Rh_xSb_{0.99}Sn_{0.01}$ half-Heusler alloys and all phases crystallize with the MgAgAs crystal structure. The diffraction peaks of the synthesized half-Heusler phases shift towards low 2θ angle with increasing Rh concentration. This trend is consistent with the substitution of small Co (1.253 Å) atoms by larger Rh (1.345 Å) atoms within the structure of $Zr_{0.5}Hf_{0.5}Co_{1-x}Rh_xSb_{0.99}Sn_{0.01}$. The unit cell parameter, a, refined from X-ray powder diffraction patterns increases almost linearly with increasing Rh concentration (Fig. 1B). Likewise, the density of polycrystalline powders of the synthesized half-Heusler alloys also increases linearly with increasing Rh concentration indicating (according to Vegard's law) the formation of "true" solid solution between the $Zr_{0.5}Hf_{0.5}CoSb_{0.99}Sn_{0.01}$ and $Zr_{0.5}Hf_{0.5}RhSb_{0.99}Sn_{0.01}$ end members. The diffraction patterns of some compositions showed additional peaks which were identified as ZrO_2 and/or HfO_2 impurities phases. Since ZrO_2 and/or HfO_2 impurity phases are not present in all samples and also because the amount of impurity is independent of the composition of the half-Heusler phase, we considered that ZrO_2 and/or HfO_2 impurities are formed as a result of the regrinding process after the first heating cycle. To avoid the formation of these impurity phases the second heating cycle was eliminated by mixing the starting materials for several hours follow by longer annealing time (up to five days) at 1173 K.

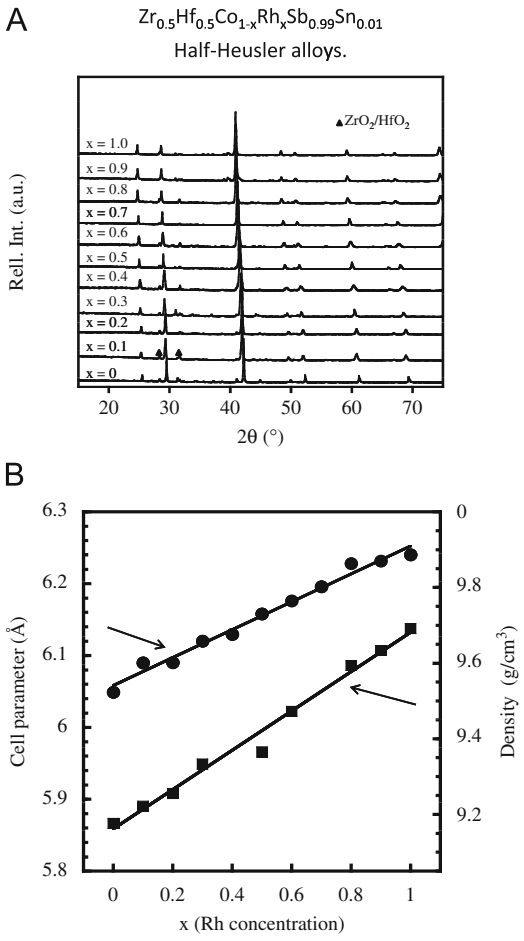

Fig. 1. (A) X-ray powder diffraction patterns of $Zr_{0.5}Hf_{0.5}Co_{1-x}Rh_xSb_{0.99}Sn_{0.01}$ ($0 \le x \le 1$) half-Heusler alloys showing clear shift of diffraction peaks towards low 2θ with increasing Rh concentration. (B) Refined unit cell parameter and measured powder density of $Zr_{0.5}Hf_{0.5}Co_{1-x}Rh_xSb_{0.99}Sn_{0.01}$ ($0 \le x \le 1$) half-Heusler alloys as a function of Rh concentration. The almost linear relationship of both parameters with varying Rh content indicates adherence to Vegard's law for solid solutions.

Fig. 2A shows the transmission electron microscopy (TEM) images of specimens prepared from a hot-pressed pellet with composition $Zr_{0.5}Hf_{0.5}Co_{0.4}Rh_{0.6}Sb_{0.99}Sn_{0.01}$. Grain sizes are in the range of 80–175 nm suggesting that half-Heusler powder materials with considerably smaller grain sizes were achieved via the high-temperature solid state reaction. The grains are densely packed and are uniform with respect to composition. A selected area electron diffraction (SAED) pattern taken from one of the grains (Fig. 2B) was indexed as the half-Heusler structure with lattice parameter $a \approx 6.10$ Å. The composition of selected specimens used for the thermoelectric properties measurements as estimated from EDS analysis, is consistent with the nominal composition. However, accurate determination of the amount of Sn by this method was not possible because of the its very small quantity and also similar transition energies of the L shell in Sb and Sn, partly overlapped which complicates the identification of trace amounts of Sn in an Sb-rich matrix. Fig. 2C shows a bright field transmission electron microscopy (TEM) image taken from a very local region of the specimen where smaller grain sizes in the range of 20–100 nm were observed. EDS analysis from the region marked by an arrow on Fig. 2C reveals the particle to be rich in Hf and oxygen compared to the matrix. This suggests that the impurity phase in the synthesized half-Heusler materials is likely HfO_2. An interface between the half- Heusler matrix and another precipitate was also observed in this specimen and was imaged at high magnification (Fig. 2D). Energy dispersive spectrum (EDS) were recorded from the half-Heusler grain matrix and from the precipitate as shown in Fig. 2E. From the analysis of the EDS spectrum, it can be seen that the precipitate is rich in Hf as compared to the grain of half-Heusler matrix. The Hf-rich precipitate is incoherently embedded in the half-Heusler grain matrix as can be observed from the HRTEM image (Fig. 2D).

Fig. 3A shows the temperature dependence of the lattice thermal conductivity of $Zr_{0.5}Hf_{0.5}Co_{1-x}Rh_xSb_{0.99}Sn_{0.01}$ samples. At 300 K, the lattice thermal conductivity of the Rh "free" composition, $Zr_{0.5}Hf_{0.5}CoSb_{0.99}Sn_{0.01}$ ($x=0$) is ~6.5 W/mK. This value is lower than the numbers reported for ZrCoSb (~9 W/mK) and HfCoSb (~7 W/mK) [21] suggesting effective phonon scattering due to mass fluctuation induced by the solid solution alloying between $ZrCoSb_{0.99}Sn_{0.01}$ and $HfCoSb_{0.99}Sn_{0.01}$. Although, the observed reduction in the lattice thermal conductivity of $Zr_{0.5}Hf_{0.5}CoSb_{0.99}Sn_{0.01}$ is significant, further reduction can be achieved upon Rh substitution at the Co site. The room temperature value of the lattice thermal conductivity of $Zr_{0.5}Hf_{0.5}Co_{1-x}Rh_xSb_{0.99}Sn_{0.01}$ decreases with increasing Rh concentration from 6.5 W/mK for $x=0$ to ~3.7 W/mK for $x=1.0$. The deviation from this general trend observed for composition $x=0.2$, which showed anomalously low lattice thermal conductivity, is presumably due to the poor compaction of the pellet (relative density = 90%).

Regardless of the temperature, the lattice thermal conductivity of $Zr_{0.5}Hf_{0.5}Co_{1-x}Rh_xSb_{0.99}Sn_{0.01}$ samples gradually decreases with increasing Rh concentration (Fig. 3B). The lattice thermal conductivity value as low as 3.7 W/mK was observed at 300 K for

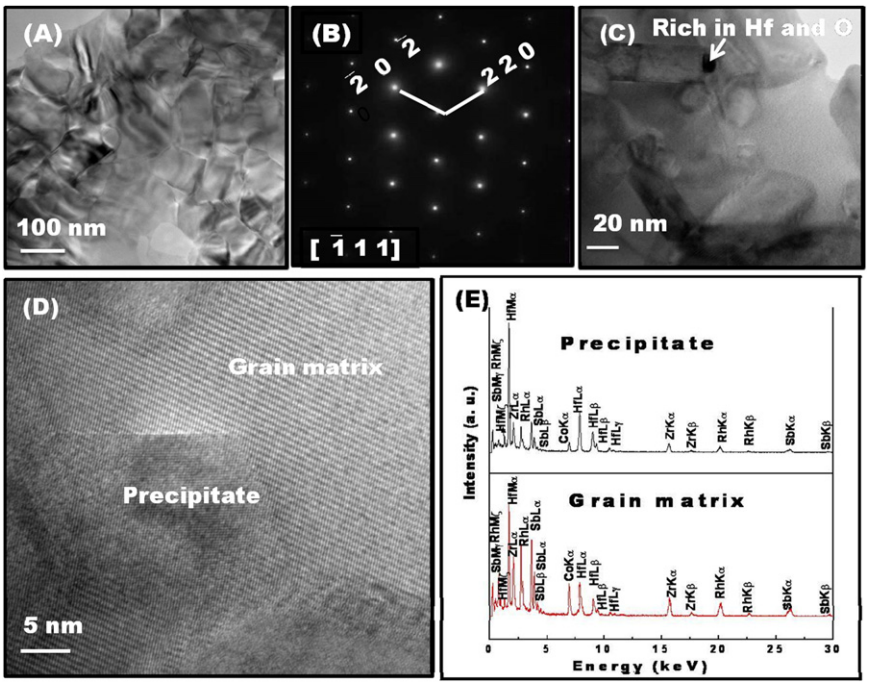

Fig. 2. (A) Bright field TEM image of $Zr_{0.5}Hf_{0.5}Co_{0.4}Rh_{0.6}Sb_{0.99}Sn_{0.01}$ specimen showing densely packed particles with grain sizes in the range from 80 to 175 nm; (B) corresponding SAED pattern along [$\bar{1}$ 1 1] zone axis of half-Heusler *fcc* phase with lattice parameter, $a=6.1$ Å obtained from the composition $Zr_{0.5}Hf_{0.5}Co_{0.4}Rh_{0.6}Sb_{0.99}Sn_{0.01}$. (C) Bright field image taken from a very local region of the specimen showing an impurity phase marked by an arrow; (D) HRTEM image showing another precipitate incoherently embedded in the half-Heusler matrix. (E) EDS analysis of the precipitate (in Fig. 2D) showing Hf-rich composition compared to the half-Heusler matrix.

$Zr_{0.5}Hf_{0.5}RhSb_{0.99}Sn_{0.01}$ ($x=1$). This corresponds to about a 40% reduction of the lattice thermal conductivity of $Zr_{0.5}Hf_{0.5}CoSb_{0.99}Sn_{0.01}$ ($x=0$). The observed drastic reduction in the lattice thermal conductivity of $Zr_{0.5}Hf_{0.5}CoSb_{0.99}Sn_{0.01}$ with increasing Rh content strongly indicates that mass fluctuation phonon scattering in ZrCoSb or HfCoSb half-Heusler phases is highly effective when substitution is operated at the Co site, compared to when the substitution involves Zr or Sb site [17–19]. In addition, because of the small grain size of the synthesized polycrystalline $Zr_{0.5}Hf_{0.5}Co_{1-x}Rh_xSb_{0.99}Sn_{0.01}$ materials (Fig. 2A), a high density of grain boundaries is expected. This also translates into enhanced phonon scattering at grain boundaries which contributes significantly to the reduction of the lattice thermal conductivity. Regardless of the composition, the lattice thermal conductivity decreases monotonically with rising temperature (Fig. 3A) and lattice thermal conductivity as low as 2.7 W/mK was achieved at 775 K for composition with $x=0.9$. A similar trend was observed for the total thermal conductivity of all $Zr_{0.5}Hf_{0.5}Co_{1-x}Rh_xSb_{0.99}Sn_{0.01}$ compounds (Fig. 3C). The difference between the total thermal conductivity and the lattice contribution is marginal for all samples due to the very low electronic thermal conductivity of $Zr_{0.5}Hf_{0.5}Co_{1-x}Rh_xSb_{0.99}Sn_{0.01}$ alloys (Fig. 3D).

Fig. 4A shows the temperature dependence of the electrical conductivity of $Zr_{0.5}Hf_{0.5}Co_{1-x}Rh_xSb_{0.99}Sn_{0.01}$ alloys. The electrical conductivity of the Rh "free" composition ($x=0$) starts at ~5 S/cm at 300 K and does not exceed 25 S/cm at 775 K. The observed temperature dependence as well as the magnitude of the electrical conductivity of the $Zr_{0.5}Hf_{0.5}CoSb_{0.99}Sn_{0.01}$ composition is consistent with compensated narrow band gap semiconductors [22,23]. Holes supplied by ~1%Sn doping on the Sb site compensate *n*-type carriers in $Zr_{0.5}Hf_{0.5}CoSb$ leading to a significant reduction of the electrical conductivity. Interestingly, Rh substitutions at the Co site significantly increase the electrical conductivity of the resulting $Zr_{0.5}Hf_{0.5}Co_{1-x}Rh_xSb_{0.99}Sn_{0.01}$ alloys. Room temperature values of the electrical conductivity gradually increase from 29 S/cm for $x=0.2$–90 S/cm (Fig. 4A) for the fully substituted alloy ($x=1$). For composition with $x=0.1$, electrical conductivity as high as ~155 S/cm was measured at 300 K. The observed dependence of the electrical conductivity on increasing Rh concentration is not yet understood. Hall Effect measurements of this series of samples are in progress to provide information on the variation of charge carriers concentration and mobility as a function of Rh concentration. The dependence of the electrical conductivity of $Zr_{0.5}Hf_{0.5}Co_{1-x}Rh_xSb_{0.99}Sn_{0.01}$ alloys on temperature strongly varies with the Rh concentration. The electrical conductivity of compositions with low Rh content ($x \leq 0.3$) is almost constant in the whole measured temperature range, while alloys with high Rh content ($x > 0.5$) show exponential increase of the electrical conductivity with temperature reaching a value of ~200 S/cm at 775 K for the $x=1$ composition. Although a significant improvement of the electrical conductivity of $Zr_{0.5}Hf_{0.5}Co_{1-x}Rh_xSb_{0.99}Sn_{0.01}$ alloys could be achieved by optimizing the Rh concentration, the observed values are still low for a promising thermoelectric material. However, the prospect of further enhancement of the electrical conductivity of this family of compounds through Sn substitution at the Sb site is very high [19].

Another surprising result of the investigation of the thermoelectric properties of $Zr_{0.5}Hf_{0.5}Co_{1-x}Rh_xSb_{0.99}Sn_{0.01}$ alloys is the notable dependence of the thermopower of the materials on Rh concentration. The Rh "free" composition $Zr_{0.5}Hf_{0.5}CoSb_{0.99}Sn_{0.01}$ exhibits *n*-type conducting behavior at all temperatures as indicated by the negative values of the thermopower (Fig. 4B). The thermopower value is about $\sim -0.5\,\mu V/K$ at 300 K and does not exceed $-10\,\mu V/K$ at higher temperatures. The observed room temperature thermopower value of $Zr_{0.5}Hf_{0.5}CoSb_{0.99}Sn_{0.01}$ is about 100 times smaller than that of $Zr_{0.5}Hf_{0.5}CoSb$ ($\sim -50\,\mu V/K$ at 300 K) [19], again suggesting compensation of *n*-type carriers in $Zr_{0.5}Hf_{0.5}CoSb$ by holes introduced with ~1% Sn substitution at the Sb site. Nevertheless, as the temperature increases, *n*-type carriers gradually became predominant in the $Zr_{0.5}Hf_{0.5}CoSb_{0.99}Sn_{0.01}$ alloy. One explanation for this behavior is the gradual population of the

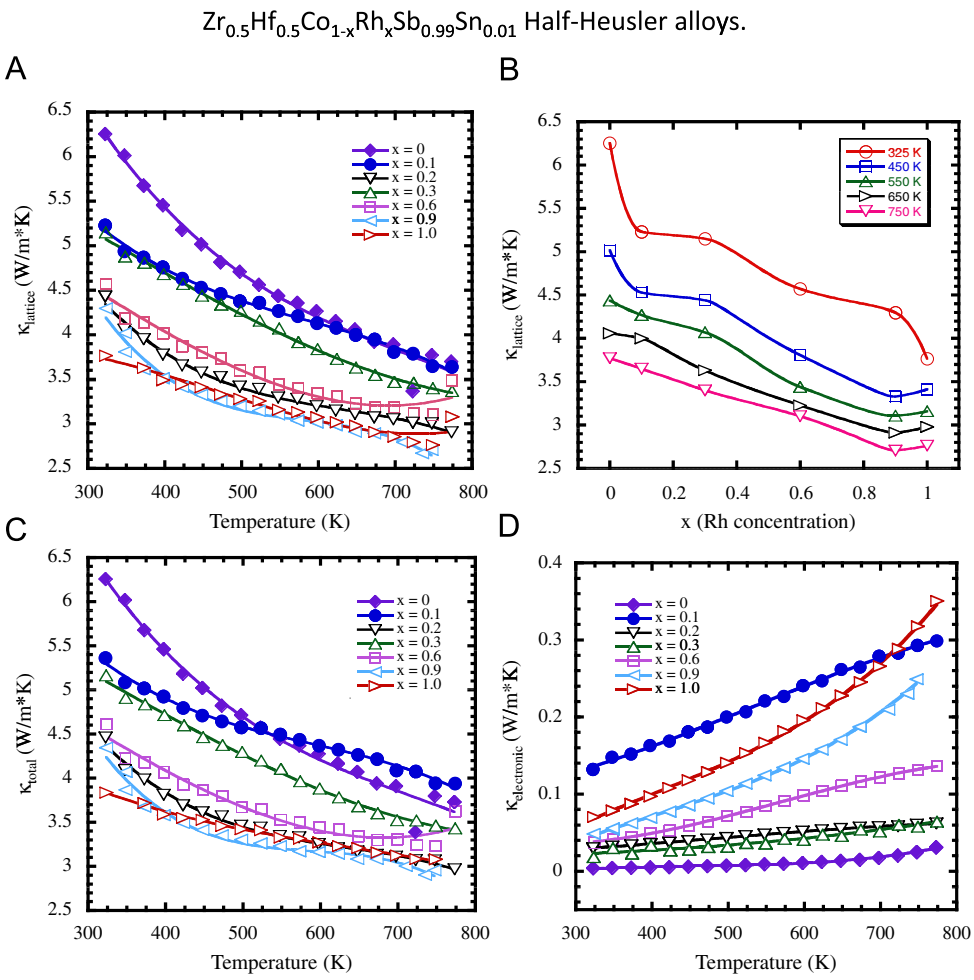

Fig. 3. (A) Temperature dependence of the lattice thermal conductivity of $Zr_{0.5}Hf_{0.5}Co_{1-x}Rh_xSb_{0.99}Sn_{0.01}$ ($0 \le x \le 1$) half-Heusler alloys. (B) Variation of the lattice thermal conductivity with increasing Rh concentration at constant temperature. Temperature dependence of the total thermal conductivity (C) and electronic thermal conductivity (D) of $Zr_{0.5}Hf_{0.5}Co_{1-x}Rh_xSb_{0.99}Sn_{0.01}$ ($0 \le x \le 1$) half-Heusler alloys.

conduction band by thermally excited electrons with rising temperature. Although Rh substitution at the Co site in the *n*-type $Zr_{0.5}Hf_{0.5}CoSb_{0.99}Sn_{0.01}$ alloy does not supply holes into the system, a small inclusion of Rh at the Co site drives the $Zr_{0.5}Hf_{0.5}Co_{1-x}Rh_xSb_{0.99}Sn_{0.01}$ system to *p*-type semiconducting behavior. The room temperature value of the thermopower slightly increases with increasing Rh concentration, reaches a maximum value of $\sim +30\,\mu V/K$ for $x=0.6$ and decreases thereafter with further addition of Rh into the system. The temperature dependence of the thermopower of $Zr_{0.5}Hf_{0.5}Co_{1-x}Rh_xSb_{0.99}Sn_{0.01}$ alloys strongly vary with Rh concentration. Although, only small differences are observed on the thermopower of various compositions at 300 K, sharp divergence is observed on thermopower curves at high temperatures. The composition $Zr_{0.5}Hf_{0.5}Co_{0.4}Rh_{0.6}Sb_{0.99}Sn_{0.01}$ ($x=0.6$) showed the strongest temperature dependence of the thermopower and a maximum value of $+135\,\mu V/K$ was observed at 775 K. The observed thermopower of $Zr_{0.5}Hf_{0.5}Co_{0.4}Rh_{0.6}Sb_{0.99}Sn_{0.01}$ is comparable to the value of $\sim +130\,\mu V/K$ at 750 K reported for the best Sn-doped half-Heusler alloy $Zr_{0.5}Hf_{0.5}CoSb_{0.8}Sn_{0.2}$ [19]. This suggests that the $Zr_{0.5}Hf_{0.5}Co_{0.4}Rh_{0.6}Sb_{0.99}Sn_{0.01}$ ($x=0.6$) composition holds great promise for enhanced figure of merit as the thermopower and electrical conductivity can be further increased via the optimization of Sn doping at the Sb site in the system. This study is currently in progress and will be reported later.

Although, large thermopower values could be achieved by optimizing the Rh concentration in the *p*-type $Zr_{0.5}Hf_{0.5}Co_{1-x}Rh_xSb_{0.99}Sn_{0.01}$ alloys, their power factors are still very low. The power factor is almost negligible at low temperatures for all samples and compositions with high Rh content ($x > 0.5$) showed a sharp increase of the power factor with rising temperature (Fig. 4C). The highest power factor, $\sim 120\,\mu W/mK^2$ at 775 K, was observed for $Zr_{0.5}Hf_{0.5}Co_{0.4}Rh_{0.6}Sb_{0.99}Sn_{0.01}$ ($x=0.6$). This composition also displays low thermal conductivity, $\sim 3.4\,W/mK$ at 775 K and the resulting dimensionless figure of merit is $ZT \sim 0.03$ at 775 K (Fig. 4D). Although, the observed figure of merit of $Zr_{0.5}Hf_{0.5}Co_{0.4}Rh_{0.6}Sb_{0.99}Sn_{0.01}$ ($x=0.6$) is low, the prospect of further increase of both the electrical conductivity and the thermopower via Sn doping at the Sb site as demonstrated in the Rh "free" compositions $Zr_{0.5}Hf_{0.5}CoSb_{1-x}Sn_x$ [19], coupled with the observed low lattice thermal conductivity make this composition ($x=0.6$) attractive in the search for high performance *p*-type thermoelectric materials for high temperature power generation.

4. Conclusions

The thermoelectric properties of several compositions of the $Zr_{0.5}Hf_{0.5}Co_{1-x}Rh_xSb_{0.99}Sn_{0.01}$ half-Heusler alloys synthesized by high temperature solid state reaction were investigated in the temperature range from 300 to 775 K. The lattice thermal conductivity of the compounds drastically decreases with increasing Rh content. Lattice thermal conductivity value of $\sim 2.7\,W/mK$ at 775 K, which is among the lowest values reported

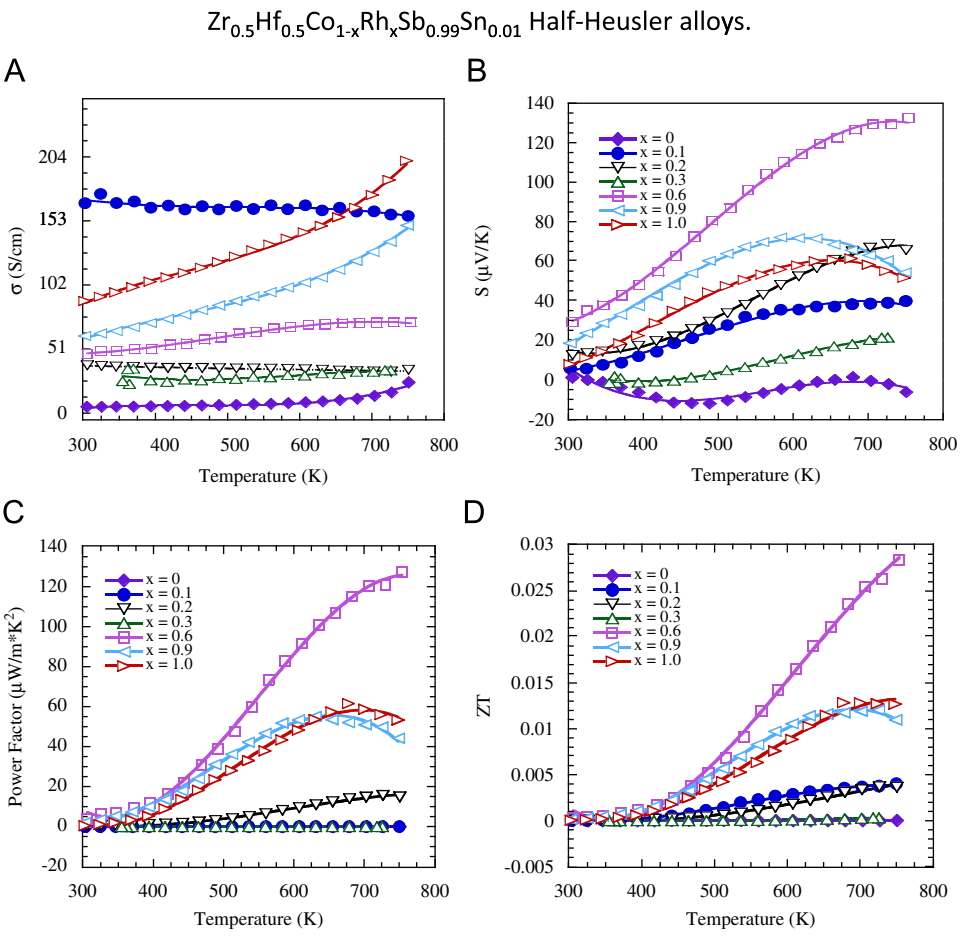

Fig. 4. Temperature dependence of: electrical conductivity (A), thermopower (B), power factor (C), and figure of merit (D) for $Zr_{0.5}Hf_{0.5}Co_{1-x}Rh_xSb_{0.99}Sn_{0.01}$ ($0 \le x \le 1$) half-Heusler alloys.

for half-Heusler compounds [4,24,25], was achieved for $Zr_{0.5}Hf_{0.5}Co_{0.1}Rh_{0.9}Sb_{0.99}Sn_{0.01}$. The drastic reduction of the lattice thermal conductivity of the $Zr_{0.5}Hf_{0.5}Co_{1-x}Rh_xSb_{0.99}Sn_{0.01}$ half-Heusler alloys is attributed to enhanced phonon scattering due to (1) high density of grain boundaries resulting from the small grain size of the synthesized materials and (2) mass fluctuation and strain fluctuation induced by Rh substitution at the Co site in $Zr_{0.5}Hf_{0.5}CoSb_{0.99}Sn_{0.01}$ system. The electrical conductivity and thermopower of $Zr_{0.5}Hf_{0.5}Co_{1-x}Rh_xSb_{0.99}Sn_{0.01}$ are very sensitive to the Rh concentration. The Rh "free" composition shows *n*-type character with low electrical conductivity and thermopower, while Rh substituted compositions exhibit positive thermopower (*p*-type) with enhanced electrical conductivity. The largest power factor of $\sim 120\,\mu W/mK^2$ at 775 K, was observed for $Zr_{0.5}Hf_{0.5}Co_{0.4}Rh_{0.6}Sb_{0.99}Sn_{0.01}$ ($x=0.6$). The dimensionless figure of merit of $Zr_{0.5}Hf_{0.5}Co_{1-x}Rh_xSb_{0.99}Sn_{0.01}$ half-Heusler alloys is enhanced by Rh substitution at the Co site and the highest value, $ZT \sim 0.03$ was observed at 775 K for $Zr_{0.5}Hf_{0.5}Co_{0.4}Rh_{0.6}Sb_{0.99}Sn_{0.01}$ ($x=0.6$). Although the observed *ZT* value is low for a viable thermoelectric material, further improvement is expected through enhancement of the electrical conductivity and thermopower via optimization of Sn doping at the Sb site. This study is underway and will be reported later.

Acknowledgments

This work was supported by DARPA under grant number HR0011-08-1-0084 awarded to the Advanced Materials Research Institute (AMRI). This work made use of the laser flash diffusivity apparatus (Netzsch-LFA457) purchased with funds from the Louisiana Board of Regents (Grant # LEQSF(2008-09)-ENH-TR-58).

References

[1] J.R. Sootsman, D.-Y. Chung, M.G. Kanatzidis, Angew. Chem. Int. Ed. 48 (2009) 8616–8639.
[2] F.J. Disalvo, Science (1999) 703–706.
[3] S.R. Culp, S.J. Poon, N. Hickman, T.M. Tritt, J. Blumm, Appl. Phys. Lett. 88 (2006) 042106/1–042106/3.
[4] C. Uher, J. Yang, S. Hu, D.T. Morelli, G.P. Meisner, Phys. Rev. B 59 (1999) 8615–8621.
[5] S.J. Poon, in: T.M. Tritt (Ed.), Semiconductors and Semimetals, Academic Press, New York, 2001, pp. 37–76.
[6] Q. Shen, L. Chen, T. Goto, T. Hirai, J. Yang, G.P. Meisner, C. Uher, Appl. Phys. Lett. 79 (2001) 4165–4167.
[7] J. Yang, G.P. Meisner, L. Chen, Appl. Phys. Lett. 85 (2004) 1140–1142.
[8] C. Yu, T.-J. Zhu, R.-Z. Shi, Y. Zhang, X.-B. Zhao, J. He, Acta Mater. 57 (2009) 2757–2764.
[9] S.R. Culp, J.W. Simonson, S.J. Poon, V. Ponnambalam, J. Edwards, T.M. Tritt, Appl. Phys. Lett. 93 (2008) 022105.
[10] Y. Xia, S. Bhattacharya, V. Ponnambalam, A.L. Pope, S.J. Poon, T.M. Tritt, J. Appl. Phys. 88 (2000) 1952.
[11] K. Kawano, K. Kurosaki, T. Sekimoto, H. Muta, S. Yamanaka, Appl. Phys. Lett. 91 (2007) 062115.
[12] B.A. Cook, J.L. Harringa, J. Mater. Sci. 34 (1999) 323.
[13] K. Mastronardi, D. Young, C.-C. Wang, P. Khalifah, R.J. Cava, A.P. Ramirez, Appl. Phys. Lett. 74 (1999) 1415.
[14] T. Sekimoto, K. Kurosaki, H. Muta, S. Yamanaka, J. Appl. Phys. 99 (2006) 103701.
[15] S. Sportouch, P. Larson, M. Bastea, P. Brazis, J. Ireland, C.R. Kannewarf, S.D. Mahanti, C. Uher, M.G. Kanatzidis, in: T.M. Tritt, M.G. Kanatzidis, G.D. Mahan, H.B. Lyon, Jr. (Eds.), Thermoelectric Materials 1998—The Next Generation Materials for Small-Scale Refrigerationand Power Generation

Applications, MRS Symposia Proceedings, Vol. 545, Materials Research Society, Pittsburgh, 1999, p. 421.
[16] T. Sekimoto, K. Kurosaki, H. Muta, S. Yamanaka, J. Alloys Compd. 407 (2006) 326.
[17] Y. Kawaharada, K. Kurosaki, H. Muta, M. Uno, S. Yamanaka, J.Alloys Compd. 384 (2004) 308.
[18] V. Ponnambalam, P.N. Alboni, J. Edwards, T.M. Tritt, S.R. Culp, S.J. Poon, J. Appl. Phys. 103 (2008) 063716.
[19] S.R. Culp, J.W. Simonson, S.J. Poon, V. Ponnambalam, J. Edwards, T.M. Tritt, Appl. Phys. Lett. 93 (2008) 022105.
[20] M. Zhou, L.D. Chen, W.Q. Zhang, C.D. Feng, J. Appl. Phys. 98 (2005) 013708.
[21] Y. Kawaharada, K. Kurosaki, H. Muta, M. Uno, S. Yamanaka, J. Alloys Compd. 384 (2004) 308.
[22] J. Yang, D.T. Morelli, G.P. Meisner, W. Chen, J.S. Dyck, C. Uher, Phys. Rev. B 67 (2003) 165207.
[23] T. Sekimoto, K. Kurosaki, H. Muta, S. Yamanaka, Int. Conf. Thermoelectrics (2005) 335.
[24] H. Hohl, A.P. Ramirez, C. Goldmann, G. Ernst, B. Woelfing, E. Bucher, J. Phys.: Condens. Matter 11 (1999) 1697.
[25] D.P. Young, P. Khalifah, R.J. Cava, A.P. Ramirez, J. Appl. Phys. 87 (2000) 317.